Environmental Nanotechnology, Monitoring & Management 20 (2023) 100826

Contents lists available at ScienceDirect

Environmental Nanotechnology, Monitoring & Management

journal homepage: www.elsevier.com/locate/enmm

Comparison of adsorption performance of nanocomposite materials of whey protein nanofibrils, polycaprolactone and activated carbon for mercury removal

Laura Cristina Ramírez-Rodríguez [a], Didilia Ileana Mendoza-Castillo [b,c], Adrián Bonilla-Petriciolet [c], Carlos Jiménez-Junca [d,*]

[a] Maestría en Diseño y Gestión de Procesos Facultad de Ingeniería, Campus Universitario Puente del Común, Universidad de la Sabana, Km. 7 Autopista Norte, 140013 Chía, Colombia
[b] Cátedras CONACYT, Instituto Tecnológico de Aguascalientes, Avenida Adolfo López Mateos #1801, Aguascalientes 20256, Mexico
[c] Departamento de Ingeniería Química, Instituto Tecnológico de Aguascalientes, Aguascalientes 20256, Mexico
[d] Bioprospecting Research Group, Campus Universitario Puente del Común, Universidad de La Sabana, Km. 7 Autopista Norte, 140013 Chía, Colombia

ARTICLE INFO

Keywords:
Adsorption
Nanocomposites
Mercury
Water depollution
Whey protein

ABSTRACT

This study reports the preparation and comparison of the mercury adsorption properties of nanocomposite materials based on whey protein. The adsorption capacity of the nanocomposites of whey protein fibrils (WPF) with activated carbon (AC) and WPF with polycaprolactone (PCL) were compared and analyzed. These materials were characterized by SEM-EDX, FTIR, and XPS. The maximum mercury adsorption capacities were 74.4, 54.7, and 16.7 mg/g for AC, WPF-AC, and WPF-PCL nanocomposites, respectively, at 30 °C and pH 5. The adsorption capacity increased with the temperature, and this thermodynamic behavior confirmed the endothermic nature of the mercury adsorption on tested materials. The results reported in this study open the possibility to use WPF to remove mercury from polluted water, which is a promising low-cost raw material to prepare a wide variety of nanocomposite materials for different industrial and environmental applications.

1. Introduction

Water is the most indispensable natural resource due to it is a source of life, where only 2% of the total water worldwide is freshwater and 1.6% of it is sealed up in polar ice caps and glaciers (Igibah et al., 2019). Therefore, the contamination of water is a global concern and one of the most important environmental pollution problems is related to the presence of heavy metal ions in industrial effluents, wastewater, and groundwater. These environmental pollutants have a massive effect on the ecosystem due to their bioaccumulation and biomagnification in the organisms and food chain (Alam et al., 2018). Consequently, several health and environmental problems are related to heavy metal contamination owing to their toxicity, carcinogenicity properties, and long-term accumulation (Azimi et al., 2017).

Mercury (Hg) has been associated with a serious concern in terms of its impact on all living organisms and the environment due to its high toxicity, volatility, and bioaccumulation. Thus, the WHO (Attari et al., 2017) and the US EPA (Monjane-Mabuie et al., 2022) have listed Hg as a priority pollutant. As a result, a maximum contamination level (MCL) of 0.2 and 1 μg/L of Hg in drinking water has been established by the US EPA (Monjane-Mabuie et al., 2022) and European Union (Bhatt and Padmaj, 2019), respectively. Similarly, the US EPA stated that the Hg amount discharged in wastewater should be below 5 μg/L (Bhatt and Padmaj, 2019). Hg discharge in wastewater higher than the limit established for its residual concentrations can cause irreversible harm to the environment. The release of Hg is the main source of mercury pollution via the emissions from mining, fossil fuel burning, and industrial production. The Hg concentration in these emissions must be controlled effectively to reduce the environmental release of this pollutant and to avoid adverse effects on ecosystems and the human population (Landin-Sandoval et al., 2020).

There are several methods to remove heavy metal ions from wastewater, including chemical precipitation, ion exchange, reverse osmosis, coagulation, and flocculation (Saleh et al., 2022). The major problems to implement these techniques for the removal of heavy metals are associated with their high cost and the demanding process to eliminate waste

* Corresponding author.
E-mail address: carlosjj@unisabana.edu.co (C. Jiménez-Junca).

https://doi.org/10.1016/j.enmm.2023.100826
Received 15 February 2023; Received in revised form 23 April 2023; Accepted 10 May 2023
Available online 13 May 2023

byproducts (Carolin et al., 2017). Researchers have focused on the adsorption technique to remove heavy metals from wastewater due to its high performance, simplicity, affordability, and versatility (Masoumi et al., 2022). The properties of adsorbents are fundamental in the removal of heavy metals; therefore, it should be identified the preparation conditions to tailor the surface area, pore size distribution, and functional groups of the adsorbent for obtaining a high adsorption capacity (Carolin et al., 2017). Adsorption is a favorable separation process because it is cost-effective, has a simple design and operation, can be used in both batch and continuous modes, and the adsorbents can be regenerated. There is a wide variety of inexpensive and effective adsorbents available from biological and chemical sources, including waste biomass (Xu et al., 2022), biochar (Hsu et al., 2021), microorganisms (Baran et al., 2020), graphene oxide composites (Awad et al., 2021), metal–organic frameworks (Soroush et al., 2022), magnetic nanocomposites (Selvaraj et al., 2023), carbon-based (Al-Yaari and Saleh, 2022) and polymer-based materials (Mahmoodi et al., 2021) that have been used to adsorb contaminants from water. Recently, the use of nanoparticles, nanocomposites, and metal–organic-frameworks has gained attention for adsorbent materials.

A promising technology for the preparation of new adsorbents is the use of protein amyloids, which are nanoscale fibers that can be used to enhance the affinity of several materials for heavy metal removal. An amyloid is a fibrillar state of a protein that can be formed under certain conditions when they are denatured (Knowles and Mezzenga, 2016). The ability of protein amyloids to remove metal ions is supported by medical evidence suggesting that metal bonds have implications in the formation of amyloid fibrils in neurodegenerative diseases (Morris and Serpell, 2010). Researchers have explored the potential role of amyloid fibrils in the removal of toxic heavy metal ions. In one study, amyloid fibrils of β-lactoglobulin produced by heat treatment with activated carbon were able to remove more than 99.5% of gold, mercury, lead, and palladium individually and mixed (Bolisetty and Mezzenga, 2016). Additionally, using the same type of membrane, 99% of arsenites and arsenates were removed from prepared solutions and contaminated real water (Bolisetty et al., 2017). Numerous studies have confirmed the promising potential of amyloids to remove heavy metals from water, but most of these reports prepared amyloid fibrils from isolated proteins such as β-Lactoglobulin and BSA using a thermal treatment method (Mezzenga et al., 2019; Peydayesh et al., 2019; Yu et al., 2019; Q. Zhang et al., 2020). In this study, we used whey protein as a source to prepare the Whey Protein Fibrils (WPF) amyloid type, which is a subproduct of the cheese industry. In consequence, whey is a mixture of proteins that could be used as a way to avoid the separation of β-lactoglobulin or other proteins, which results in lower-cost production. It is important to remark that the use of whey to produce nanocomposites based on WPF is promissory to remove heavy metals from water due to its chemical characteristics, and low cost. Herein, it is convenient to note that the mechanical and physical properties of amyloids make them difficult to handle alone and, consequently, several studies have used support to hold amyloids with the aim of preparing nanocomposite materials (Li et al., 2012). The application of nanotechnology in wastewater treatment for toxic heavy metal ions using nanocomposites has taken great relevance, which has many advantages owing to the combination of the properties of the nanoscale, components, and the strong economic incentives (Saad et al., 2018). In consequence, activated carbon has been used to support whey protein and β-Lactoglobulin amyloids and the resulting nanocomposite material has proved to remove efficiently heavy metals from water (Bolisetty and Mezzenga, 2016; Ramírez-Rodríguez et al., 2020). Activated carbon provides mechanical support to amyloids and it is a well-known adsorbent owing to its large surface area but due to its synthesis cost, a nanocomposite material is preferred because of the combination of a low-cost material as whey with activated carbon (Wang et al., 2022).

Similarly, nanocomposite-based adsorbents made of nanofibers produced by electrospinning have been receiving widespread attention due to the advantages of their high efficiency, simple production, versatility, large specific surface area, high porosity, and good structural stability (Damiri et al., 2022). Electrospinning is a method that allows the production of ultrathin nanofibers that can be manufactured under controlled conditions leading to fibers with desirable properties (Kumar et al., 2018). This is an opportunity to make amyloid-like fibers by an innovative method using a polymer as a mechanical support besides activated carbon, thus avoiding the use of the thermal treatment method to produce the amyloid fibers. Note that the thermal treatment is a method commonly used to obtain amyloid fibers but the fibrillar arrangement depends on the denaturation conditions of the protein, so that spherulites or gels may form, which are well-known that do not have an affinity for heavy metals (Zappone et al., 2013). Therefore, there is the opportunity to use an affordable raw material such as whey to produce amyloid fibrils by thermal treatment at low temperatures and electrospinning and to elaborate different nanocomposite materials for the removal of metal ions. Recently, Ramírez-Rodríguez et al. reported the preparation of a hybrid membrane made of whey protein fibrils and activated carbon to remove Hg and chromium from water, thus demonstrating the potential use of whey to prepare amyloids for heavy metals removal (Ramírez-Rodríguez et al., 2020). It is important to remark that the adsorption performance of the nanocomposites of WPF-PCL has not been evaluated in the literature before for mercury removal.

The aim of this study was to compare the adsorption behavior of nanocomposite materials based on whey protein fibrils and determine their benefits with respect to the non-modified materials (i.e., activated carbon and polycaprolactone) to remove Hg ions from water. WPF were prepared by a thermal treatment which is the most used method, while fibrils were incorporated into activated carbon (AC) structure to elaborate a nanocomposite material. The performance of this adsorbent was compared with a nanocomposite of WPF and polycaprolactone (PCL) made by the electrospinning process. Hg adsorption properties of these nanocomposite adsorbents and non-modified materials were analyzed. This study demonstrated that whey protein fibrils in the amyloid state have a high affinity for mercury and this has been proven through the incorporation of these fibers in different materials such as activated carbon and PCL. The novelty of this research is focused on the adsorption performance of nanocomposites based on WPF, which serves as a tool to enhance the Hg affinity of other compounds. The results of this study can be considered as an important contribution in the nanocomposite materials area, where amyloids can be used in conjunction with other materials to elaborate new and cost-effective promising adsorbents for different industrial and environmental applications.

2. Experimental

2.1. Materials

Whey Protein Isolated (WPI) was purchased from Davisco Foods International Inc. (Eden Prairie, USA) and it contained 97% protein (69% β-Lactoglobulin and 22% α-lactalbumin), activated carbon was obtained from Sigma Aldrich (USA) with a particle size of 150 μm. Poly (epsilon-caprolactone) (PCL, Mn = 70–90 kDa) was obtained from Sigma Aldrich (USA), and 2-Mercaptoethanol (βME, 98%) was purchased from Bio-Rad Laboratories (Canada). Mercury chloride (II) was obtained from Sigma Aldrich (USA).

2.2. Preparation of nanocomposite adsorbents

2.2.1. Nanocomposite adsorbent based on WPF and AC

Whey powder was dissolved in deionized water at a concentration of 3.8% at pH 2 to ensure fibril formation owing to the electrostatic repulsion among positively charged groups (Loveday et al., 2017). The solution was centrifuged at 10,800 RFC for 1 h using a Centrifuge (Universal 32R, Germany), and filtered with a 0.45 μm millipore filter. The solution was placed in glass tubes in a water bath without stirring at

74 °C for 7 h, and the tubes were immediately cooled by immersion in ice-water mixtures as reported previously (Ramírez-Rodríguez et al., 2020). The nanocomposite adsorbent was prepared using the WPF solution, which was dropped into an AC solution (0.1 wt%) to obtain a final mixture 1:2 of AC–WPF. This solution was stirred at 200 rpm and 20 °C for 24 h to ensure the incorporation of WPF into the AC.

2.2.2. Nanocomposite adsorbent based on WPF and PCL

Polymeric dispersions of WPI and PCL were prepared using a concentration of total solids of 18% with concentrations of WPI at 90% wt, PCL at 10% wt, and 1.0% v/v of 2-Mercaptoethanol (βME), which was used as reducing agent to denature whey proteins from a native state to amyloid state (Aceituno-Medina et al., 2013). Solutions of PCL and WPI with βME were dissolved in tetrahydrofuran (THF) and dimethyl formamide (DMF) (7:3 v/v) separately and stirred overnight at room temperature to ensure complete dissolution. To produce the nanocomposite adsorbent, a solution of WPI and PCL was pumped by a horizontal electrospinning Fluidnatek ® LE-10 (Bioinicia, Spain) apparatus as reported previously (Ramírez-Rodríguez et al., 2022). To facilitate the adsorption essays, the film was cut and washed with ethanol (10%) and HNO_3 (0.1 N) for 24 h under continuous stirring.

2.3. Mercury adsorption studies using nanocomposite adsorbents and non-modified materials

Adsorption studies were conducted using aqueous solutions of mercury chloride. Batch experiments were done by triplicate using an adsorbent - adsorbate solution ratio of 20 g/L at 120 rpm. Prior to the experiment, a stock aqueous solution of mercury chloride was adjusted to the desired pH using 0.1 M of HNO_3. Hg concentration was quantified using an Atomic Absorption Spectrophotometer ContrAA 700 (Analytik Jena, Germany) with a linear calibration curve (i.e., 10–300 mg/L). The adsorption capacity (q, mg/g) of the nanocomposite adsorbents was calculated using a mass balance that is given by Eq. (1) (Zúñiga-Muro et al., 2020):

$$q = \frac{(C_i - C_f)V}{m} \tag{1}$$

where C_i and C_f are the initial and final mercury concentrations in the solution (mg/L), V is the volume of mercury solution (L) and m is the adsorbent mass (g), respectively.

Adsorption kinetic studies were performed at 30 °C and pH 2 using initial Hg concentrations of 50 and 150 mg/L with contact times from 1 to 18 h. The adsorption data were fitted to classical adsorption kinetic models and the calculation of the adsorption rate constants was made using a nonlinear data regression (see Table S1). Adsorption isotherms were obtained at different conditions of pH (2–5) and temperature (20 and 30 °C) with initial Hg concentrations from 10 to 300 mg/L using an equilibrium time of 24 h. The experimental isotherms were fitted to Langmuir, Freundlich, and Sips models (see Table S2). The thermodynamic parameters of the mercury adsorption process were calculated using the Gibbs free energy (ΔG°, kJ/mol), Eq. (2), and the standard enthalpy (ΔH°) and entropy (ΔS°) of the nanocomposite adsorbents were calculated using van't Hoff approach, Eq. (3).

$$\Delta G = -RTlnK_c \tag{2}$$

$$lnK_c = \frac{-\Delta H^{\circ}}{RT} + \frac{\Delta S^{\circ}}{R} \tag{3}$$

where the adsorption equilibrium constant was calculated according to (Lima et al., 2020; Tran et al., 2017).

2.4. Physicochemical characterization of nanocomposite adsorbents and non-modified materials

Physicochemical characterization of nanocomposite adsorbents and the non-modified materials was performed via the quantification of the pH of the point of zero charge (PZC), the morphology analysis was done using SEM-EDX and the surface chemistry analysis with FTIR and XPS techniques. The zero charge pH (pH_{pzc}) of the adsorbents was determined by employing the methodology reported by Faria et al. (2004). The morphology of the adsorbents was observed by a Scanning Electron Microscopy (SEM) JEOL JSM 5910 LV (Joel, Japan) equipped with an Energy-Dispersive X-ray spectrometer (EDX), model 7324 (Oxford Instruments, UK) at an acceleration voltage of 10 kV (Yu et al., 2019). Functional groups of the adsorbent samples were identified by FTIR spectroscopy using a Nicolet iS10 spectrometer (Thermo Scientific®, USA) equipped with a DTGS detector at a resolution of 4 cm^{-1} and 32 scans. FTIR analysis was done using KBr pellets in the range of 4000–400 cm^{-1} (Mahmoodi et al., 2019). XPS characterization was done with a Centeno-XPS/ISS/UPS X-Ray Photoelectron Spectrometer (SPECS, Germany) where the spectra were recorded using monochromatic Al Kα radiation (hv = 1486.6 eV), and the data analysis was performed with the CasaXPS program (Casa Software Ltd).

2.5. Statistical analysis

All statistical analyses were done using SPSS software version 17.0. Analysis of variance (ANOVA) was conducted to determine the differences between treatments. Significant differences were established with Fisher's test with a significance level of 0.05. All the experiments were carried out in triplicate, and the results were reported as the mean and standard deviation of the measurements.

3. Results and discussion

3.1. Characterization of the nanocomposite adsorbents and non-modified materials

3.1.1. SEM-EDX Analysis

SEM results for the surface morphology analysis of AC, WPF-AC, and WPF-PCL nanocomposite materials are reported in Figs. 1 and 2. SEM images of Fig. 1A and 2A show the heterogeneous surface and porous nature of AC, where porous of different diameters were observed. Similarly, the micrographs of the nanocomposite adsorbent of WPF-AC (see Fig. 1B and 2B) showed a heterogeneous surface due to the high composition of AC. Note that the WPF could be incorporated mainly in the micropores and macropores of AC due to WPF have a diameter of 5 nm and their length may vary from 2 nm to 1 μm (Knowles and Mezzenga, 2016; Ramírez-Rodríguez et al., 2020). In this case, the presence of micropores and mesopores on the adsorbent surface is desired where a high specific surface area of the material is expected to favor the adsorption of heavy metals (Yan et al., 2020).

On the other hand, the SEM characterization of the WPF-PCL nanocomposite adsorbent demonstrated that this material was made of nanofibrils with a diameter of 62.2 nm (see Fig. 2C), beadles, and with the presence of some micropores. This result indicated that the adsorbent besides having ultra-thin fibers that increased its specific surface area, it also contained some micropores that increased the surface area to favor its adsorption properties. The presence of micropores was also evidenced by Martins et al. that identified the presence of micropores in 37% of fibers elaborated with PCL (Martins et al., 2015). A similar finding was observed by Ahmed et al. that prepared fiber of WPI and PCL for an antibiotic release with a porosity of 80% (Ahmed et al., 2016). The presence of micropores on the fibers was due to the high solvent evaporation rate during the electrospinning process or owing to the humidity of the electrospinning space caused by the vapor-induced phase separation mechanism (Jiang et al., 2018).

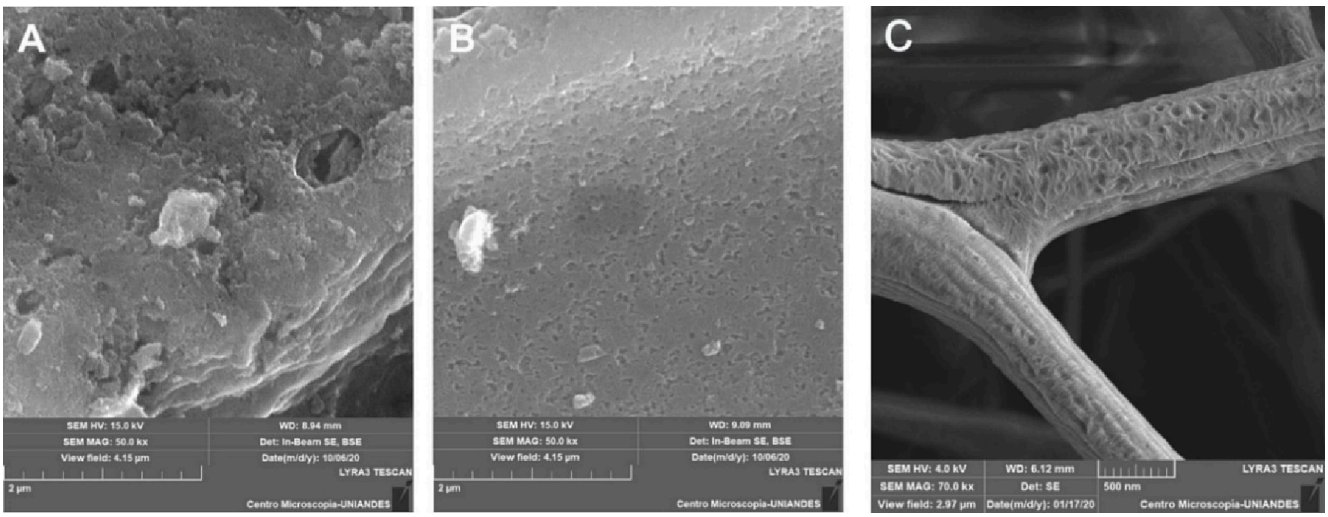

Fig. 1. SEM images of A) Activated carbon at 50 kx, the nanocomposites of B) WPF-AC at 50 kx and C) WPF-PCL at 70 kx.

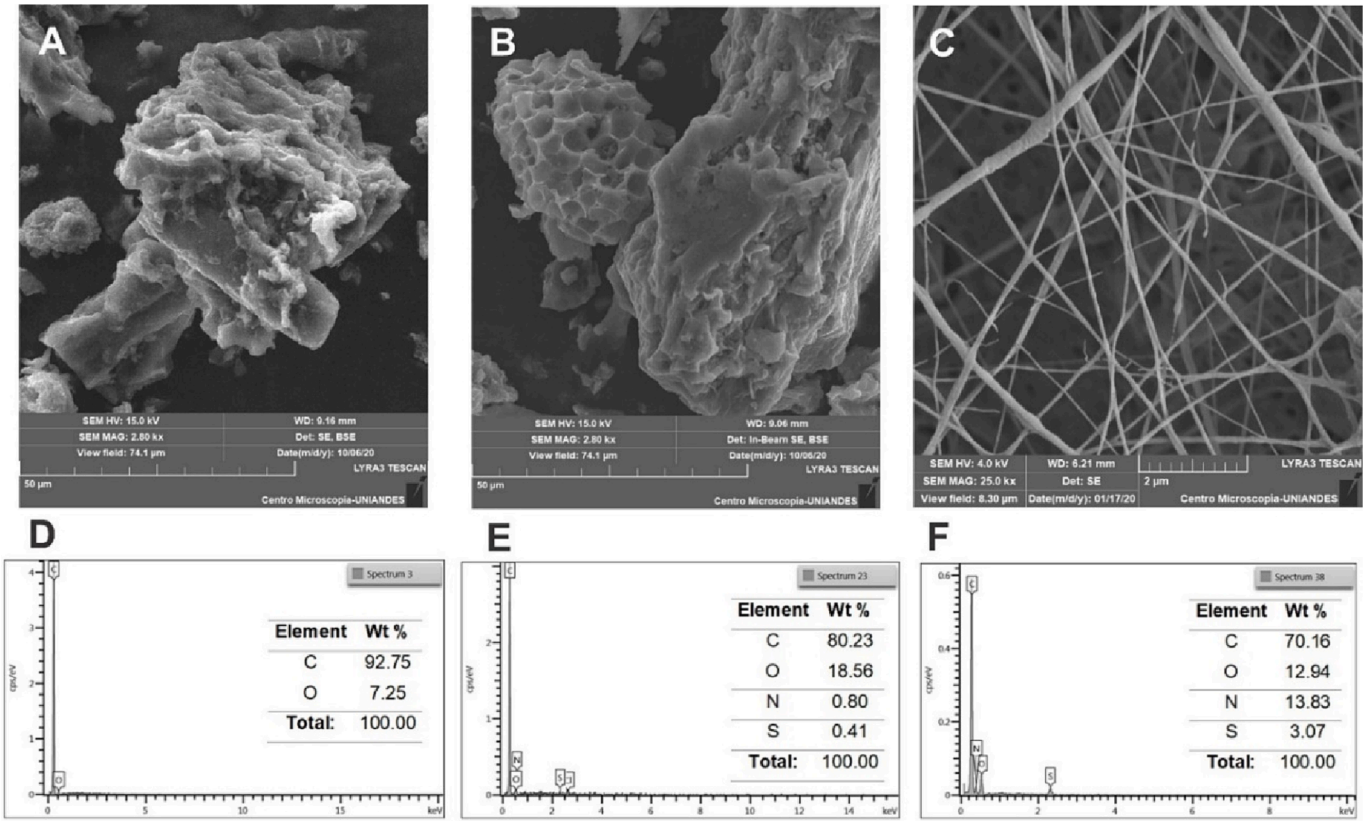

Fig. 2. SEM maps and EDX analysis of A,D) Activated carbon at 2.8 kx, the hybrids of B,E) WPF-AC at 2.8 kx and C,F) WPF-PCL at 25 kx.

SEM-EDX analysis were carried out on the AC sample alone and in the WPF-AC and WPF-PCL nanocomposite adsorbents, see Fig. 2. EDX analysis showed that AC was composed of carbon at 92% and oxygen at 7.2% and this result was consistent with the study reported by Rengga et al (2017). Similarly, SEM-EDX analysis of the WPF-AC nanocomposite material demonstrated that it was composed mainly of carbon and oxygen, but it also contained nitrogen and sulfur, which were characteristic elements of whey proteins (Yan et al., 2020). In contrast, the EDX analysis of WPF-PCL nanocomposite sample showed that it was composed mainly of 70% of carbon besides oxygen, nitrogen, and sulfur, which were the main elements of whey proteins and PCL. In this way, it can be concluded that the WPF nanocomposite adsorbents showed a porous morphology and the characteristic elements of whey protein thus making them promissory to adsorb Hg from water.

3.1.2. FTIR analysis

FTIR spectra results of the characterization WPI, AC, PCL, and nanocomposite adsorbents before adsorption are reported in Fig. 3. The results showed that the WPF-AC (blue line) and WPF-PCL (green line) nanocomposites contained the functional groups of their main components. The spectrum of WPF-AC nanocomposite displayed the characteristic functional groups of the whey proteins related to peptide bonds

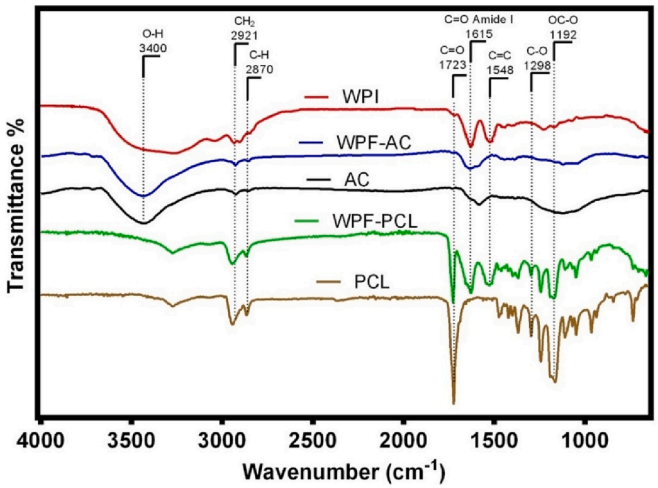

Fig. 3. FTIR spectra of WPI, AC, PCL, and the WPF-AC and WPF-PCL nanocomposite adsorbents.

In the case of the WPF-PCL nanocomposite, the FTIR spectra showed that it also had the main functional groups of whey proteins such as primary (1615 cm^{-1}) and secondary (1548 cm^{-1}) amide groups and the corresponding absorption bands were more intense in WPF-PCL than those of the WPF-AC nanocomposite due to its higher amount of WPI (O'Loughlin et al., 2015). Also, the WPF-PCL sample presented the characteristic ester band at 1723 cm^{-1}, the bands of CH_2 asymmetric and symmetric vibrations at 2921 and 2870 cm^{-1}, the C–O and C–C stretching bands at 1298 cm^{-1} (Azizi et al., 2018), the asymmetric C–O–C stretching band at 1246 cm^{-1} and the symmetric C–O–C stretching band at 1192 cm^{-1} of PCL, which were similar to the results reported by other researchers (Li et al., 2018). Finally, it was concluded that the nanocomposites obtained in this study showed the main functional groups of whey protein, so that; it could be expected a similar performance of the nanocomposites compared to amyloids for the Hg adsorption due to the high affinity of whey proteins by heavy metals (Bolisetty and Mezzenga, 2016).

such as the primary amide group (1615 cm^{-1}) (Colín-Orozco et al., 2014) and the C-N bond stretching vibrations in the range of 1350–1380 cm^{-1} (Nagalakshmi et al., 2015). It presented the characteristic absorption bands of methylene of AC at 2921 cm^{-1} for the asymmetric stretching and the band at 1600 cm^{-1} related to the aromatic C = C ring stretching vibration (Mojoudi et al., 2019). FTIR spectra of WPI (red line) and WPF-AC nanocomposite showed an absorption band at 3400 cm^{-1} that corresponded to the stretching vibrations of –OH linked to $–NH_2$ (Gbassi et al., 2012), and it can be also attributed to a hydroxyl carboxylic and phenolic group of AC (Merodio-Morales et al., 2020).

3.2. Adsorption performance of the nanocomposite adsorbents

3.2.1. Adsorption kinetics

Hg adsorption kinetics of AC, PCL, and the WPF-AC and WPF-PCL nanocomposite adsorbents at 30 °C and pH 2 are shown in Fig. 4. There was a rapid increase of Hg uptake in the initial phase due to the abundant vacant adsorption sites of these adsorbents. Thereafter, the adsorption capacity slowed down as the equilibrium was achieved and almost became constant after 3 h for WPF-PCL, 4 h for AC, and WPF-AC, while PCL did not show a Hg adsorption capacity at any time. As indicated, the pseudo-first order (PFO), pseudo-second order (PSO), and intraparticle diffusion models were applied to analyze the adsorption data and to study the Hg kinetics.

These results indicated that the materials followed the PSO model (see Table 1), which showed the best R^2 values than those obtained with PFO and intraparticle diffusion models, see Table S3. Note that PSO model assumes that two surface adsorption sites will be occupied by one adsorbate ion such as C-C/C = O, –OH, NHC = O functional groups (Bullen et al., 2021; Rajamohan et al., 2014). Consequently, these results demonstrated that the rate-limited step in all the studied adsorbents was the adsorption process instead of the diffusion process (Hubbe et al., 2019).

Hg adsorption rates ranged from 0.07 to 0.23 mg/min for AC thus being slightly higher than the adsorption rates of WPF-AC

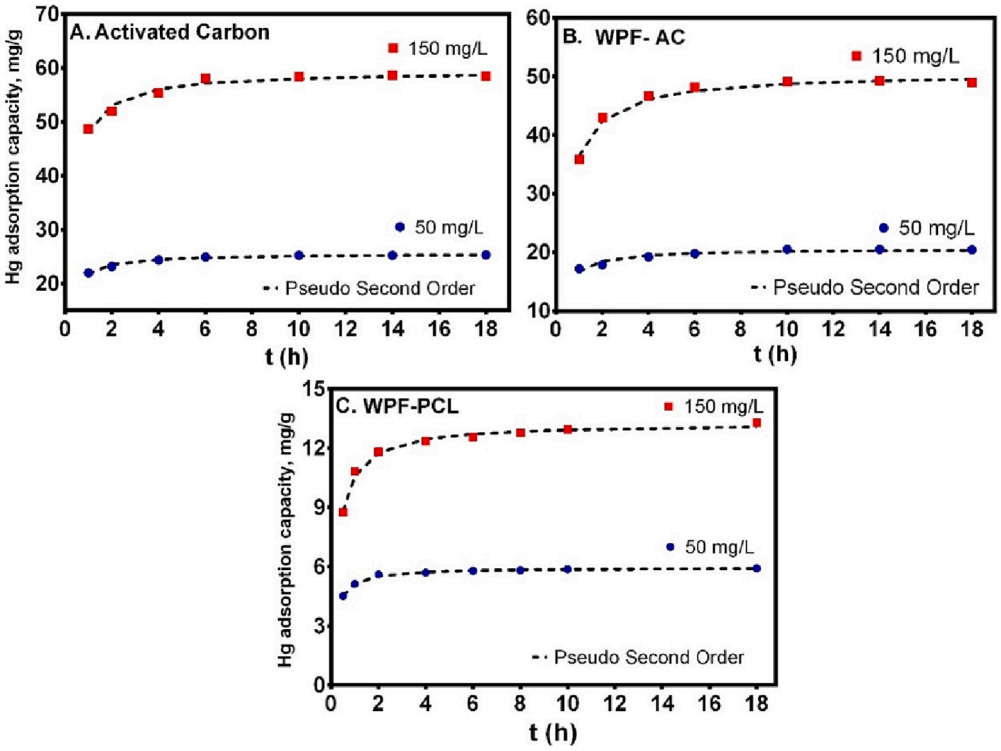

Fig. 4. Kinetics for the Hg adsorption on A) AC and the nanocomposite adsorbents of B) WPF-AC and C) WPF-PCL at 30 °C and pH 2. Hg initial concentrations of 50 and 150 mg/L.

Table 1
Parameter of the Pseudo Second Order kinetic model for the adsorption of mercury using AC, WPF-AC and WPF-PCL adsorbents.

Adsorbent	Initial Hg concentration, mg/L	PSO kinetic parameters q_{te} (mg/g)	K_2 (mg/min)	R^2
Activated Carbon	50	25.51	0.23	0.98
	150	59.42	0.07	0.97
Nanocomposite WPF-AC	50	20.58	0.21	0.95
	150	50.61	0.05	0.98
Nanocomposite WPF-PCL	50	5.95	1.07	0.99
	150	13.24	0.30	0.99

nanocomposite adsorbent, which were 0.05 and 0.21 mg/min. The adsorption rate of the WPF-PCL sample (i.e., 0.3–1.07 mg/min) was higher than those calculated for the other tested adsorbents, which may be due to the difference in the surface area of these materials. In this case, the carbonaceous-based materials had a specific surface area ranging from 400 to 600 m^2/g and the WPF-PCL adsorbent had a specific surface area of 2 m^2/g, which explained that the adsorption rate of WPF-PCL was higher than those of AC and WPF-AC. As reported in the literature, carbonaceous bio-based materials reported a specific surface area between 12 to 363 m^2/g, which depends on the nature of the adsorbent and the synthesis process (Kumar et al., 2020; Saleh et al., 2017). On the other hand, some authors report the specific surface area of the nanocomposite materials based on nanofibers, which vary from 2 to 21 m^2/g due to the morphology and materials of the fibers made by the electrospinning process (Asadollahfardi et al., 2018). The differences between the adsorption performance within the composites maybe be due to the differences in the specific surface area which is a valuable factor in the adsorption process.

3.2.2. *Adsorption isotherms and thermodynamic parameters*

Hg adsorption isotherms of AC and the WPF-AC and WPF-PCL nanocomposite adsorbents are reported in Fig. 5. All isotherms were regular, positive, and concave with respect to the concentration axis, and they can be classed as L2 type isotherm of Giles classification, which corresponded to a favorable adsorption process in a liquid phase (Giles et al., 1960). The adsorption isotherms at different pH of AC and the WPF-AC and WPF-PCL nanocomposite adsorbents are given in Fig. 4A, 4B, and 4C, respectively. These results showed that the adsorption capacity increased with the increase of pH in all tested materials, where pH 5 was the best to remove Hg obtaining adsorption capacities of 74.4 mg/g for AC, 54.7 mg/g for the WPF-AC nanocomposite and 16.7 mg/g for the WPF-PCL nanocomposite. The change in the pH solution caused the deprotonation or protonation of different functional groups of these adsorbents (Zúñiga-Muro et al., 2020), which depended on the PZC pH of these materials (Tran et al., 2017).

The PZC values of AC, PCL, and the WPF-AC and WPF-PCL nanocomposites were: pH 5.2, 3.5, 3.6, and 3.0, respectively. The differences between the PZC pH of the nanocomposites and AC or PCL were associated with the content of WPF, where the main proteins of whey such as α-lactalbumin and β-lactoglobulin added acidic groups to AC or PCL during the preparation of the nanocomposite materials (Heidemann et al., 2019). Considering that the surface of these materials was negatively charged at pH > PZC pH, this explained the increase of the Hg removal with the increase of solution pH where the electrostatic interactions were the main forces leading the adsorption process (Hamad et al., 2020). Furthermore, note that the concentration of H^+ ions in the solution depended on the pH solution and, consequently, Hg species competed with H^+ at acidic conditions thus reducing the adsorption capacities of tested adsorbents (Mortazavian et al., 2019).

The effect of temperature on the adsorption capacity of AC and the WPF-AC and WPF-PCL nanocomposite adsorbents is illustrated in Fig. 4D, 4E, and 4F, respectively. It was clear that the temperature promoted the adsorption capacity, where the adsorption capacities increased from 20 to 30 °C at 30%, 7%, and 8 % for WPF-PCL, WPF-AC, and AC, respectively. The increase of the adsorption capacity as a function of solution temperature was due to the increment of the mobility of Hg ions in the solution thus promoting their interaction with the main adsorption receptor sites on the surface of these adsorbents (Li et al., 2020).

The classical Langmuir, Freundlich, and Sips equations were used to

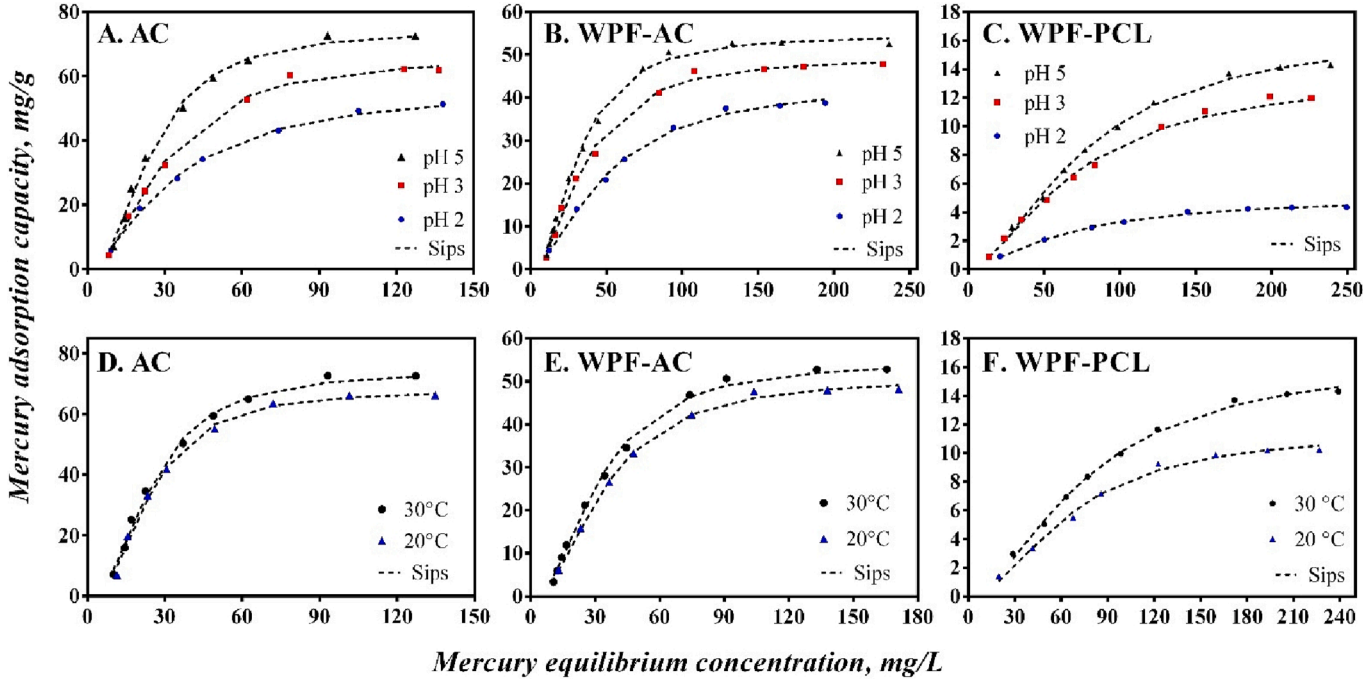

Fig. 5. Adsorption isotherms for the removal of Hg using A) Activated Carbon, B) the WPF-AC hybrid adsorbent and C) the WPF-PCL hybrid adsorbent. A, B, C) 30 °C and different pH; D,E,F) pH 5 and different temperature.

analyze the adsorption equilibrium data, see Table S4. The Sips model was the best to correlate the experimental data (see Table 2) with $R^2 > 0.96$ and modeling errors < 8%. Sips equation is an isotherm model that includes the features of Langmuir and Freundlich models. At low concentrations, the Sips model can be reduced to the Freundlich isotherm, and it can predict a monolayer adsorption capacity characteristic of the Langmuir isotherm at higher concentrations (Aguayo-Villarreal et al., 2011).

The heterogeneity factor (n_s) of Sips model usually is associated with the heterogeneity of the surface sites that carry out the adsorption process. For instance, $n_s = 1$ indicates that the adsorbent surface is homogeneous, and the Sips model is reduced to Langmuir model, while if n_s differs significantly from 1, it indicates that the adsorbent will have a greater surface heterogeneity (Guimarães et al., 2016). The results demonstrated that n_s increased with the solution pH suggesting that the surface heterogeneity increased with pH during the mercury adsorption with all evaluated materials. This could happen because the charge of the functional groups on the tested materials changed with the increase in solution pH (Franz et al., 2000).

On the other hand, the results demonstrated that the removal performance of all tested adsorbents increased with the increase in temperature revealing the temperature-dependent nature of the Hg adsorption process (Tran et al., 2017). These results indicated that the Hg adsorption was an endothermic process where the estimated enthalpies were 4.64, 3.43, and 2.15 kJ/mol using WPF-AC, AC, and WPF-PCL respectively, see Table 3. According to Aguayo-Villarreal et al., an enthalpy changes from 2 to 21 kJ/mol is owing to a physical adsorption process and, consequently, it can be concluded that the Hg adsorption in tested materials may be related to a physisorption process (Aguayo-Villarreal et al., 2011; Liu and Liu, 2008). Also, the Gibbs free energy presented a negative value, which suggested that this adsorption process was spontaneous and more energetically favorable with the increase in solution temperature (Maleki et al., 2016). Furthermore, the calculated entropy for all studied cases was positive indicating the increase of randomness at the solid/solution interface during the adsorption process (Liu and Liu, 2008).

The maximum adsorption capacities obtained in this study for the WPF-AC and WPF-PCL nanocomposite adsorbents were 54.7 and 16.7 mg/g, respectively, at pH 2 and 30 °C. The adsorption capacity of the nanocomposite materials was compared with other composite materials reported in the literature, see Table 4. WPF-AC nanocomposite sample presented better Hg adsorption properties compared to the composite materials of polyethylenimine modified-activated carbon (Saleh et al., 2017), algal biomass bioadsorbent (Kumar et al., 2020), and the bio-originated composite B–CA–NaOH (Amiri et al., 2018). However, the polyacrylate-modified carbon composite showed an adsorption capacity of 76.30 mg/g which was 40% higher than the Hg removal of the WPF-AC nanocomposite sample. In these studies, the authors also concluded that Hg adsorption was associated with electrostatic interactions and surface complexation, which played a key role to remove Hg ions from an aqueous solution (Al-Yaari and Saleh, 2022). On the other hand, the comparison of the adsorption performance of the WPF-PCL nanocomposite sample with other nanocomposite membranes obtained by electrospinning indicated that its adsorption capacity was highly competitive with respect to the membranes of copper ferrite nanofibers (Asadollahfardi et al., 2018) and Fe-modified montmorillonite particles in polycaprolactone (Raj Somera et al., 2019) that showed Hg adsorption capacities of 0.03 and 14 mg/g, see Table 4. Also, it was identified that some membranes produced by electrospinning showed higher adsorption capacities than those of the adsorbents reported in this study (Alosaimi, 2021; Zou et al., 2017). For example, the poly(2-aminothiazole)/cellulose acetate fiber membrane had an adsorption capacity of 177 mg/g (Zou et al., 2017), but it required an equilibrium time of 12 h, which was significantly higher than the equilibrium time of samples tested in this study (i.e., 3 h). Note that the operating time reported in this paper is advantageous for a large-scale application because low contact times are required to intensify the water treatment process.

Table 2
Results of data correlation of Sips model for the adsorption of Hg on AC, WPF-AC and WPF-PCL adsorbents.

Adsorbent	T (°C)	pH	Sips q_s (mg/g)	K_s (L^{ns}/mg^{ns})	n_s	R^2
Activated Carbon	30	2	56.76	0.030	1.53	0.99
		3	66.20	0.034	1.96	0.99
		5	74.37	0.040	2.21	0.99
	20	5	67.98	0.041	2.31	0.99
Nanocomposite WPF-AC	30	2	43.78	0.020	1.64	0.99
		3	49.44	0.028	1.96	0.99
		5	54.73	0.031	2.08	0.99
	20	5	50.90	0.029	2.07	0.99
Nanocomposite WPF-PCL	30	2	5.12	0.015	1.42	0.99
		3	13.72	0.014	1.62	0.99
		5	16.72	0.013	1.71	0.99
	20	5	11.53	0.015	1.89	0.99

Table 3
Calculated thermodynamic parameters for the mercury adsorption on the AC, WPF-AC, and WPF-PCL nanocomposite adsorbents.

Adsorbent	T (°C)	ΔG°, kJ/mol	ΔH°, kJ/mol	ΔS°, kJ/mol K
AC	20	−1.6	3.43	0.02
	30	−1.8		
Nanocomposite WPF-AC	20	−0.1	4.64	0.02
	30	−0.3		
Nanocomposite WPF-PCL	20	−0.6	2.15	0.01
	30	−0.7		

3.3. Adsorption mechanism of the nanocomposite adsorbents

Results of FT-IR spectra and XPS analysis were utilized to understand and explain the interaction mechanism between Hg ions and tested materials. After Hg adsorption, some changes were observed in the FTIR spectrum (see Fig. 6) of the WPF-PCL nanocomposite (dark red line). In particular, the intensity of absorption bands located at 1719 (C = O), 1553 (Amide I), 1530 (–CO-NH), and 1229–1000 cm^{-1} was reduced thus indicating the role of these functional groups in the Hg removal. These results agreed with the findings of Zhang et al. (S. Zhang et al., 2020). For the WPF-AC nanocomposite and AC samples, the intensity of bands at 2908 (symmetric vibrations) and 2810 cm^{-1} (asymmetric vibrations) of the methylene group (CH_2) was strengthened, and new bands appeared between 1615 and 780 cm^{-1} that were related to oxygen-containing functional groups. This result was also evidence of the ligand exchange between Hg ions and the oxygen- and nitrogen-containing functional groups on the adsorbent structure (Guo et al., 2020).

XPS spectra before and after Hg adsorption of AC and WPF-AC and WPF-PCL nanocomposites are shown in the survey spectra of Fig. 7. The survey spectra displayed the peaks of O 1 s, C 1 s, for AC, WPF-AC, and WPF-PCL. N1 s peak was identified in the spectra of WPF-AC (11.28%) and WPF-PCL (4.37%), and traces of the S 2p peak were observed in these samples confirming the protein composition of WPF in the nanocomposite materials (see Table S5). Also, Hg 4f peak was clearly identified in all tested materials after Hg adsorption, which was evidence to verify the adsorption of Hg ions on the adsorbent surfaces.

The high-resolution XPS spectra for C 1 s (see Fig. S1) was deconvoluted into three peaks consisting of C-C/C-H (284.8 eV), C-O/C-N (285.6 eV), and C = O (288.5 eV). The intensity of these peaks slightly changed after Hg adsorption on nanocomposite materials, which could

Table 4
Comparison of adsorption capacities of different composite adsorbents used in mercury removal from water.

Adsorbent	qe (mg/g)	pH	Temperature	Area (m^2/g)	Equilibrium time	Reference
Copper ferrite nanofiber in polyvinylpyrrlidone	0.03	7.5	25 °C	21	–	(Asadollahfardi et al., 2018)
Fe- modified montmorillonite particles in polycaprolactone	14.25	3	–	–	3 h	(Raj Somera et al., 2019)
Polyethylenimine modified-activated carbon	16.39	5	25 °C	363	4 h	(Saleh et al., 2017)
Algal biomass	42.10	6	35 °C	12	1.5 h	(Kumar et al., 2020)
Bio-originated composite B–CA–NaOH	45.34	5.5	25 °C	17	0.5 h	(Amiri et al., 2018)
Silica nanoparticles with 1-hydroxy-2 acetonaphthone composite	50.94	6.5	25 °C	89	1.5 h	(Al-Wasidi et al., 2022)
Polyacrylate-modified carbon composite	76.30	6	65 °C	348	1.5 h	(Al-Yaari and Saleh, 2022)
Polysulfone Membrane Hybrid Nanocomposite (PSF/MMt/CNTOxi)	151.36	2	25 °C	–	–	(Alosaimi, 2021)
Poly(2-aminothiazole) /cellulose acetate composite	177.00	6.5	25 °C	–	12 h	(Zou et al., 2017)
Nanocomposite WPF-AC	54.73	5	30 °C	595	4 h	This study
Nanocomposite membrane of WPI-PCL	16.72	5	30 °C	2	3 h	

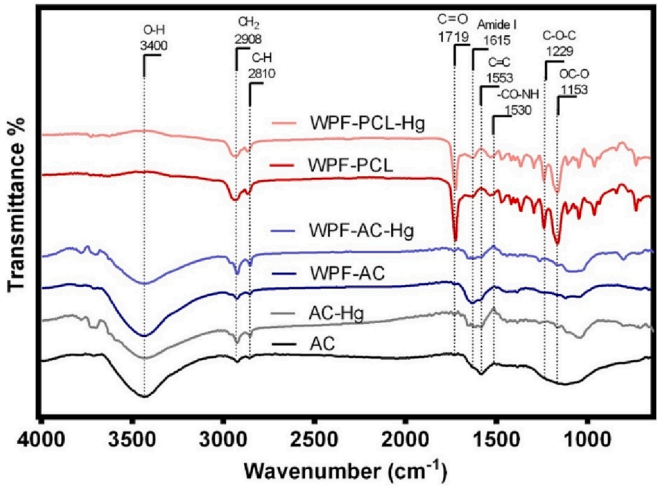

Fig. 6. FTIR spectra for AC, WPF-AC and WPF-PCL nanocomposite adsorbents after the mercury adsorption.

be due to weak interactions between C-C/C = O and Hg (Li et al., 2019; S. Zhang et al., 2020). Also, the HR XPS spectra of O 1 s (see Fig. S2) was deconvoluted into C = O (532.2 eV), C-OH (533.6 eV), and C-O (534.93) peaks. Also, significant changes were identified in the intensity of the deconvoluted peaks after Hg adsorption that may happen regarding the chemisorbed oxygen and weakly bonded oxygen species. This phenomenon could be attributed to an interaction between Hg and oxygen to form HgO as stated by some researchers (Duan et al., 2019; S. Zhang et al., 2020). Traces of Cl were observed at a peak of 198.9 eV due to Cl, which existed as HgCl. Finally, N 1 s spectra (see Fig. S3) of the nanocomposite materials was deconvoluted into NHC = O (400.7), NH_2 (400.3 eV), and NH_3 (403.8 eV) peaks. It was observed a significant change in the intensity of all peaks and the presence of NH_3 peak after the heavy metal adsorption due to the interaction of nitrogen species with Hg to coordinate as –NH-Hg^+ (Y. Zhao et al., 2019).

The results showed that the Hg removal mechanism was not simple physical adsorption as confirmed by the Hg 4f spectra (see Fig. S4) that exhibited the peaks Hg 4f 7/2 (101.5 eV) and Hg 4f 5/2 (105.5 eV). These peaks were attributed to Hg (II) ions in the form of oxides or coordination compounds according to other results reported in the literature (Schiesaro et al., 2020). Consequently, the possible removal mechanism of Hg onto the WPF-based nanocomposite materials could be summarized as shown in Fig. 8. The nanocomposite adsorbents prepared

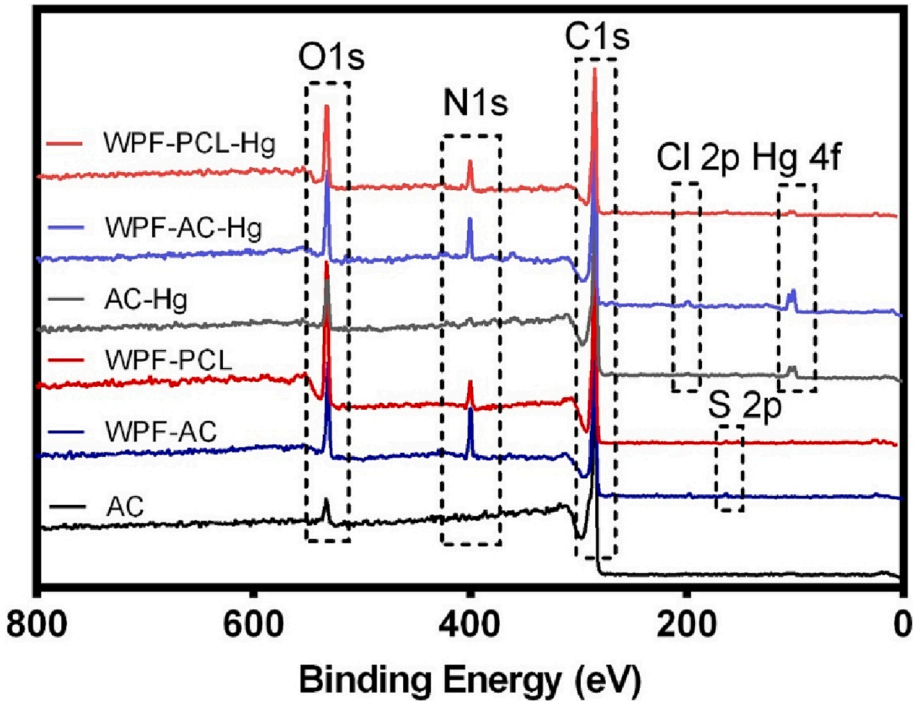

Fig. 7. XPS spectra of AC, WPF-AC and WPF-PCL hybrid adsorbents before and after the mercury adsorption.

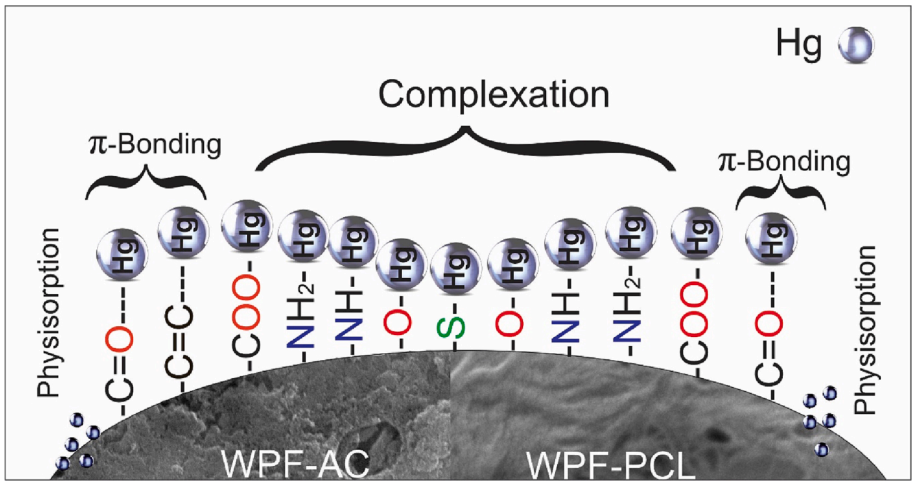

Fig. 8. Illustration of mercury adsorption mechanism for the WPF and WPF-PC nanocomposite materials.

with the whey protein could adsorb Hg ions via surface complexes interaction as -S-Hg, and between functional groups such as C-C/C = O, –OH, NHC = O (Bhatt and Padmaj, 2019; Duan et al., 2019; X. Zhao et al., 2019). Also, weak electrostatic interactions such as π-π could occur between C-C/C = O and Hg^{2+} (Li et al., 2019). Finally, the thermodynamic analysis also suggested that the physical adsorption forces could play an important role in Hg removal with WPF-AC.

4. Conclusions

This work has prepared and compared the mercury adsorption properties of two nanocomposite adsorbents based on WPF with AC and PCL, respectively. This study evaluated two different ways to produce amyloid-type fibrils with the aim of obtaining nanocomposite adsorbents using WPI to remove mercury ions, where electrospinning and thermal treatment at low temperature were used in the adsorbent synthesis. The morphological characterization results of the WPF-AC and WPF-PCL nanocomposite adsorbents allowed to conclude that these materials presented a porous morphology and ultra-thin nanofibers, respectively. These characteristics facilitated the adsorption of mercury ions on the adsorbent surfaces. The chemical characterization also showed that the nanocomposite adsorbents maintained the main functional groups of WPI, AC, and PCL. WPF-AC sample showed a better removal performance than WPF-PCL, which may be due to the amount of PCL that does not have affinity by heavy metal ions and its low surface area. However, the adsorption capacity of WPF-AC was outperformed by AC, but this WPF-AC nanocomposite material offers a strong economic incentive due to the impact of WPF on the preparation cost and the final physicochemical properties of the adsorbent.

It is important to remark that the Hg adsorption properties of WPF-AC and WPF-PCL nanocomposite materials showed the same patterns where the metal removal was favored with temperature and the best results were obtained at pH 5. Mercury adsorption mechanism was similar in both materials involving surface complexes, electrostatic interactions, and weak physical interaction forces. Both nanocomposite materials showed a good performance to remove Hg from water, which makes them suitable for different industrial and environmental applications. The nanocomposite of WPF-AC offers a significant advantage due to the collaborative effect of the functional groups of WPF and the surface area of the AC for the removal of Hg, resulting in a strong economic incentive. However, it should be noted that a disadvantage of this material is due to the reduction in surface area of the WPF-AC nanocomposite that affects its removal performance, which can be addressed by using AC with higher pore size, that way WPF won't fill the microporous of the AC and instead of that it will cover the surface of the pores.

The use of electrospinning for the elaboration of the WPF-PCL nanocomposite offers a controlled production of amyloid fibers, making it a promising method for the creation of nanocomposites. Future research should focus on evaluating new types of nanocomposites made from polymers with affinity to Hg to enhance adsorption performance. This study confirms that WPF obtained from whey, a byproduct of the cheese industry, can be used in combination with other compounds to produce novel adsorbents with high adsorption performance to remove Hg from water. The materials studied are chemically stable and inexpensive, and their production is simple and easy to implement. This context opens the possibility to use this type of amyloid fibrils made of whey protein to produce new and cost-effective adsorbents to remove heavy metals and other pollutants from water.

CRediT authorship contribution statement

Laura Cristina Ramírez-Rodríguez: Writing – original draft, Conceptualization, Methodology, Investigation. **Didilia Ileana Mendoza-Castillo:** Investigation, Formal analysis, Writing – review & editing. **Adrián Bonilla-Petriciolet:** Supervision, Writing – review & editing. **Carlos Jiménez-Junca:** Supervision, Project administration, Writing – review & editing.

Declaration of Competing Interest

The authors declare the following financial interests/personal relationships which may be considered as potential competing interests: Carlos Jimenez-Junca has patent #NC2021/0014697 pending to Superintendencia de Industria y Comercio Colombia. Carlos Jimenez-Junca has patent #NC2021/0014667 pending to Superintendencia de Industria y Comercio Colombia. Laura Cristina Ramirez-Rodriguez has patent #NC2021/0014697 pending to Superintendencia de Industria y Comercio Colombia. Laura Cristina Ramirez-Rodriguez has patent #NC2021/0014667 pending to Superintendencia de Industria y Comercio Colombia.

Data availability

Data will be made available on request.

Acknowledgements

Authors gratefully acknowledge the support of Universidad de La Sabana (ING-287-2021) and CONACYT, Instituto Tecnologico de Aguascalientes. Also, Authors acknowledge to Martha Isabel Cobo Angel

by the use of the ChemBET Pulsar TPR/TPD apparatus to carry out the BET area experiments, and María Ximena Quintanilla-Carvajal by the use of the electrospinning apparatus. Laura Cristina Ramirez-Rodriguez would personally acknowledge to Universidad de La Sabana for the Teaching Assistant Scholarship, and to the postgraduate of chemical engineering of Instituto Tecnologico de Aguascalientes for the support in her research internship.

Appendix A. Supplementary data

Supplementary data to this article can be found online at https://doi.org/10.1016/j.enmm.2023.100826.

References

Aceituno-Medina, M., Lopez-Rubio, A., Mendoza, S., Lagaron, J.M., 2013. Development of novel ultrathin structures based in amaranth (Amaranthus hypochondriacus) protein isolate through electrospinning. Food Hydrocoll. 31 (2), 289–298.

Aguayo-Villarreal, I.A., Bonilla-Petriciolet, A., Hernández-Montoya, V., Montes-Morán, M.A., Reynel-Avila, H.E., 2011. Batch and column studies of Zn2+ removal from aqueous solution using chicken feathers as sorbents. Chem. Eng. J. 167, 67–76. https://doi.org/10.1016/j.cej.2010.11.107.

Ahmed, S.M., Ahmed, H., Tian, C., Tu, Q., Guo, Y., Wang, J., 2016. Whey protein concentrate doped electrospun poly(epsilon-caprolactone) fibers for antibiotic release improvement. Colloids Surf. B Biointerfaces 143, 371–381. https://doi.org/10.1016/j.colsurfb.2016.03.059.

Alam, M., Khan, M., Khan, A., Zeb, S., Khan, M.A., Amin, N., Sajid, M., Khattak, A.M., 2018. Concentrations, dietary exposure, and human health risk assessment of heavy metals in market vegetables of Peshawar, Pakistan. J. Environ. Monit. Assess. 190–505 https://doi.org/10.1007/s10661-018-6881-2.

Alosaimi, A.M., 2021. Polysulfone membranes based hybrid nanocomposites for the adsorptive removal of Hg (II) ions. Polymers (Basel) 13 (16), 2792.

Al-Wasidi, A.S., Naglah, A.M., Saad, F.A., Abdelrahman, E.A., 2022. Modification of silica nanoparticles with 1-hydroxy-2-acetonaphthone as a novel composite for the efficient removal of Ni(II), Cu(II), Zn(II), and Hg(II) ions from aqueous media. Arab. J. Chem. 15 (8), 104010.

Al-Yaari, M., Saleh, T.A., 2022. Mercury Removal from Water Using a Novel Composite of Polyacrylate-Modified Carbon. ACS Omega 7, 14820–14831. https://doi.org/10.1021/ACSOMEGA.2C00274.

Amiri, M.J., Arshadi, M., Giannakopoulos, E., Kalavrouziotis, I.K., 2018. Removal of Mercury (II) and Lead (II) from Aqueous Media by Using a Green Adsorbent: Kinetics, Thermodynamic, and Mechanism Studies. J. Hazard. Toxic Radioact. Waste 22, 04017026. https://doi.org/10.1061/(asce)hz.2153-5515.0000383.

Asadollahfardi, G., Naseraei, M.M., Asadi, M., Alizadeh, R., 2018. The study of mercury removal using synthesized copper ferrite nanofiber in laboratory scale. Environ. Nanotechnol. Monit. Manag. 10, 79–86. https://doi.org/10.1016/j.enmm.2018.05.007.

Attari, M., Bukhari, S.S., Kazemian, H., Rohani, S., 2017. A low-cost adsorbent from coal fly ash for mercury removal from industrial wastewater. J. Environ. Chem. Eng. 5, 391–399. https://doi.org/10.1016/j.jece.2016.12.014.

Awad, F.S., AbouZied, K.M., Bakry, A.M., Abou El-Maaty, W.M., El-Wakil, A.M., El-Shall, M.S., 2021. Polyacrylonitrile modified partially reduced graphene oxide composites for the extraction of Hg(II) ions from polluted water. J. Mater. Sci. 56, 7982–7999. https://doi.org/10.1007/S10853-021-05797-2/TABLES/5.

Azimi, A., Azari, A., Rezakazemi, M., Ansarpour, M., 2017. Removal of Heavy Metals from Industrial Wastewaters: A Review. ChemBioEng Rev. 4, 37–59. https://doi.org/10.1002/cben.201600010.

Azizi, M., Azimzadeh, M., Afzali, M., Alafzadeh, M., Mirhosseini, S.H., 2018. Characterization and Optimization of Using Calendula Officinalis Extract in The Fabrication of Polycaprolactone/Gelatin Electrospun Nanofibers for Wound Dressing Applications. J. Adv. Mater. Process. 6, 34–46.

Baran, M.F., Yildirim, A., Acay, H., Keskin, C., Aygun, H., 2020. Adsorption performance of Bacillus licheniformis sp. bacteria isolated from the soil of the Tigris River on mercury in aqueous solutions. https://doi-org.ez.unisabana.edu.co/10.1080/03067319.2020.1746779 102, 2013–2028. 10.1080/03067319.2020.1746779.

Bhatt, R., Padmaj, P., 2019. A chitosan-thiomer polymer for highly efficacious adsorption of mercury. Carbohydr. Polym. 207, 663–674. https://doi.org/10.1016/j.carbpol.2018.12.018.

Bolisetty, S., Mezzenga, R., 2016. Amyloid-carbon hybrid membranes for universal water purification. Nat. Nanotechnol. 11, 365–371. https://doi.org/10.1038/nnano.2015.310.

Bolisetty, S., Reinhold, N., Zeder, C., Orozco, M.N., Mezzenga, R., 2017. Efficient purification of arsenic-contaminated water using amyloid-carbon hybrid membranes. Chem. Commun. 53, 5714–5717. https://doi.org/10.1039/C7CC00406K.

Bullen, J.C., Saleesongsom, S., Gallagher, K., Weiss, D.J., 2021. A Revised Pseudo-Second-Order Kinetic Model for Adsorption, Sensitive to Changes in Adsorbate and Adsorbent Concentrations. Langmuir 37, 3189–3201. https://doi.org/10.1021/acs.langmuir.1c00142.

Carolin, C.F., Kumar, P.S., Saravanan, A., Joshiba, G.J., Naushad, M., 2017. Efficient techniques for the removal of toxic heavy metals from aquatic environment: A review. J. Environ. Chem. Eng. 5, 2782–2799. https://doi.org/10.1016/j.jece.2017.05.029.

Colín-Orozco, J., Zapata-Torres, M., Rodríguez-Gattorno, G., Pedroza-Islas, R., 2014. Properties of Poly (ethylene oxide)/ whey Protein Isolate Nanofibers Prepared by Electrospinning. Food Biophys. 10, 134–144. https://doi.org/10.1007/s11483-014-9372-1.

Damiri, F., Andra, S., Kommineni, N., Balu, S.K., Bulusu, R., Boseila, A.A., Akamo, D.O., Ahmad, Z., Khan, F.S., Rahman, M.H., Berrada, M., Cavalu, S., 2022. Recent Advances in Adsorptive Nanocomposite Membranes for Heavy Metals Ion Removal from Contaminated Water: A Comprehensive Review. Materials 15, 5392. https://doi.org/10.3390/MA15155392.

Duan, X.L., Yuan, C.G., Jing, T.T., Yuan, X.D., 2019. Removal of elemental mercury using large surface area micro-porous corn cob activated carbon by zinc chloride activation. Fuel 239, 830–840. https://doi.org/10.1016/j.fuel.2018.11.017.

Faria, P.C.C., Órfão, J.J.M., Pereira, M.F.R., 2004. Adsorption of anionic and cationic dyes on activated carbons with different surface chemistries. Water Res. 38, 2043–2052. https://doi.org/10.1016/j.watres.2004.01.034.

Franz, M., Arafat, H.A., Pinto, N.G., 2000. Effect of chemical surface heterogeneity on the adsorption mechanism of dissolved aromatics on activated carbon. Carbon N Y 38, 1807–1819. https://doi.org/10.1016/S0008-6223(00)00012-9.

Gbassi, G., Yolou, F., Sarr, S., Atheba, P., Amin, C., Ake, M., 2012. Whey proteins analysis in aqueous medium and in artificial gastric and intestinal fluids. Int. J. Biol. Chem. Sci. 6, 1828–1837. https://doi.org/10.4314/ijbcs.v6i4.38.

Giles, C.H., MacEwan, T.H., Nakhwa, S.N., Smith, D., 1960. A System of Classification of Solution Adsorption Isotherms, and its Use in Diagnosis of Adsorption Mechanisms and in Measurement of Specific Surface Areas of Solids. J. Chem. Soc. 846, 3973–3993.

Guimarães, V., Rodríguez-Castellón, E., Algarra, M., Rocha, F., Bobos, I., 2016. Influence of pH, layer charge location and crystal thickness distribution on U(VI) sorption onto heterogeneous dioctahedral smectite. J. Hazard. Mater. 317, 246–258. https://doi.org/10.1016/j.jhazmat.2016.05.060.

Guo, Z., Kang, Y., Liang, S., Zhang, J., 2020. Detection of Hg(II) in adsorption experiment by a lateral flow biosensor based on streptavidin-biotinylated DNA probes modified gold nanoparticles and smartphone reader. Environ. Pollut. 266, 115389 https://doi.org/10.1016/j.envpol.2020.115389.

Hamad, A.A., Hassouna, M.S., Shalaby, T.I., Elkady, M.F., Abd Elkawi, M.A., Hamad, H. A., 2020. Electrospun cellulose acetate nanofiber incorporated with hydroxyapatite for removal of heavy metals. Int. J. Biol. Macromol. 151, 1299–1313. https://doi.org/10.1016/j.ijbiomac.2019.10.176.

Heidemann, H.M., Dotto, M.E.R., Laurindo, J.B., Carciofi, B.A.M., Costa, C., 2019. Cold plasma treatment to improve the adhesion of cassava starch films onto PCL and PLA surface. Colloids Surf A Physicochem Eng Asp 580, 123739.

Hsu, C.-J., Cheng, Y.-H., Huang, Y.-P., Atkinson, J.D., Hsi, H.-C., 2021. A novel synthesis of sulfurized magnetic biochar for aqueous Hg(II) capture as a potential method for environmental remediation in water. Sci. Total Environ. 784, 147240 https://doi.org/10.1016/j.scitotenv.2021.147240.

Hubbe, M.A., Azizian, S., Douven, S., 2019. Implications of apparent pseudo-second-order adsorption kinetics onto cellulosic materials: A review. BioResources 14, 7582–7626. https://doi.org/10.15376/biores.14.3.7582-7626.

Igibah, E.C., Agashua, L.O., Sadiq, A.A., 2019. Water contamination: Burden and stratagems for control. J. Phys. Conf. Ser. 1378 (4), 042011.

Jiang, L., Wang, L., Wang, N., Gong, S., Wang, L., Li, Q., Shen, C., Turng, L.S., 2018. Fabrication of polycaprolactone electrospun fibers with different hierarchical structures mimicking collagen fibrils for tissue engineering scaffolds. Appl. Surf. Sci. 427, 311–325. https://doi.org/10.1016/j.apsusc.2017.08.005.

Knowles, T.P.J., Mezzenga, R., 2016. Amyloid Fibrils as Building Blocks for Natural and Artificial Functional Materials. Adv. Mater. 28, 6546–6561. https://doi.org/10.1002/adma.201505961.

Kumar, M., Singh, A.K., Sikandar, M., 2020. Biosorption of Hg (II) from aqueous solution using algal biomass: kinetics and isotherm studies. Heliyon 6 (1). https://doi.org/10.1016/j.heliyon.2020.e03321.

Kumar, P.S., Venkatesh, K., Gui, E.L., Jayaraman, S., Singh, G., Arthanareeswaran, G., 2018. Electrospun carbon nanofibers/TiO2-PAN hybrid membranes for effective removal of metal ions and cationic dye. Environ Nanotechnol Monit Manag 10, 366–376. https://doi.org/10.1016/j.enmm.2018.08.006.

Landin-Sandoval, V.J., Mendoza-Castillo, D.I., Bonilla-Petriciolet, A., Aguayo-Villarreal, I.A., Reynel-Avila, H.E., Gonzalez-Ponce, H.A., 2020. Valorization of agri-food industry wastes to prepare adsorbents for heavy metal removal from water. J. Environ. Chem. Eng. 8 (5), 104067.

Li, C., Adamcik, J., Mezzenga, R., 2012. Biodegradable nanocomposites of amyloid fibrils and graphene with shape-memory and enzyme-sensing properties. Nat. Nanotechnol. 7, 421–427. https://doi.org/10.1038/nnano.2012.62.

Li, Z., Hanafy, H., Zhang, L., Sellaoui, L., Schadeck Netto, M., Oliveira, M.L.S., Seliem, M. K., Luiz Dotto, G., Bonilla-Petriciolet, A., Li, Q., 2020. Adsorption of congo red and methylene blue dyes on an ashitaba waste and a walnut shell-based activated carbon from aqueous solutions: Experiments, characterization and physical interpretations. Chem. Eng. J. 388, 124263 https://doi.org/10.1016/j.cej.2020.124263.

Li, X., Wang, C., Yang, S., Liu, P., Zhang, B., 2018. Electrospun PCL/mupirocin and chitosan/ lidocaine hydrochloride multifunctional double layer nanofibrous scaffolds for wound dressing applications. Int. J. Nanomed. 13, 5287–5299. https://doi.org/10.2147/IJN.S177256.

Li, Y., Xia, M., An, F., Ma, N., Jiang, X., Zhu, S., Wang, D., Ma, J., 2019. Superior removal of Hg (II) ions from wastewater using hierarchically porous, functionalized carbon. J. Hazard. Mater. 371, 33–41. https://doi.org/10.1016/J.JHAZMAT.2019.02.099.

Lima, E.C., Gomes, A.A., Tran, H.N., 2020. Comparison of the nonlinear and linear forms of the van't Hoff equation for calculation of adsorption thermodynamic parameters (ΔS° and ΔH°). 10.1016/j.molliq.2020.113315.

Liu, Y., Liu, Y.J., 2008. Biosorption isotherms, kinetics and thermodynamics. Sep. Purif. Technol. 61, 229–242. https://doi.org/10.1016/j.seppur.2007.10.002.

Loveday, S., Anema, S.G., Singh, H., 2017. β-Lactoglobulin nanofibrils: The long and the short of it. Int. Dairy J. 67, 35–45. https://doi.org/10.1016/j.idairyj.2016.09.011.

Mahmoodi, N.M., Taghizadeh, A., Taghizadeh, M., AZimi Shahali Baglou, M., 2019. Surface modified montmorillonite with cationic surfactants: Preparation, characterization, and dye adsorption from aqueous solution. J. Environ. Chem. Eng. 7 (4), 103243.

Mahmoodi, N.M., Mokhtari-Shourijeh, Z., Langari, S., Naeimi, A., Hayati, B., Jalili, M., Seifpanahi-Shabani, K., 2021. Silica aerogel/polyacrylonitrile/polyvinylidene fluoride nanofiber and its ability for treatment of colored wastewater. J. Mol. Struct. 1227, 129418 https://doi.org/10.1016/J.MOLSTRUC.2020.129418.

Maleki, A., Hayati, B., Najafi, F., Gharibi, F., Joo, S.W., 2016. Heavy metal adsorption from industrial wastewater by PAMAM/TiO2 nanohybrid: Preparation, characterization and adsorption studies. J. Mol. Liq. 224, 95–104. https://doi.org/10.1016/J.MOLLIQ.2016.09.060.

Martins, A.J., Bourbon, A.I., Vicente, A.A., Pinto, S., Lopes Da Silva, J.A., Rocha, C.M.R., 2015. Physical and mass transfer properties of electrospun ε-polycaprolactone nanofiber membranes. Process Biochem. 50, 885–892. https://doi.org/10.1016/j.procbio.2015.03.017.

Masoumi, H., Ghaemi, A., Ghanadzadeh Gilani, H., 2022. Surveying the elimination of hazardous heavy metal from the multi-component systems using various sorbents: a review. Journal of Environmental Health Science and Engineering 2022 20:2 20, 1047–1087. 10.1007/S40201-022-00832-Z.

Merodio-Morales, E.E., Reynel-Ávila, H.E., Mendoza-Castillo, D.I., Duran-Valle, C.J., Bonilla-Petriciolet, A., 2020. Lanthanum- and cerium-based functionalization of chars and activated carbons for the adsorption of fluoride and arsenic ions. Int. J. Environ. Sci. Technol. 17, 115–128. https://doi.org/10.1007/s13762-019-02437-w.

Mezzenga, R., Zhang, Q., Bolisetty, S., Cao, Y., Handschin, S., Adamcik, J., 2019. Selective and efficient removal of fluoride from water by in-situ engineered amyloid fibrils-ZrO2 hybrid membranes. Angewandte Chemie - International Edition 1–66. https://doi.org/10.1002/ejoc.201403115.

Mojoudi, N., Mirghaffari, N., Soleimani, M., Shariatmadari, H., Belver, C., Bedia, J., 2019. Phenol adsorption on high microporous activated carbons prepared from oily sludge: equilibrium, kinetic and thermodynamic studies. Sci. Rep. 9, 1–12. https://doi.org/10.1038/s41598-019-55794-4.

Monjane-Mabuie, A., Mondlane-Milisse, A., Pedro, O., Leão-Buchir, J., Correia, D., 2022. Mercury pollution assessment and metallothionein gene expression in tilapia (Oreochromis mossambicus): a case study of Revuè River in Manica, Mozambique. Rendiconti Lincei 33, 513–526. https://doi.org/10.1007/S12210-022-01092-7/FIGURES/7.

Morris, K., Serpell, L., 2010. From natural to designer self-assembling biopolymers, the structural characterisation of fibrous proteins and peptides using fibre diffraction. Chem. Soc. Rev. 39, 3445. https://doi.org/10.1039/b919453n.

Mortazavian, S., Saber, A., Hong, J., Bae, J.H., Chun, D., Wong, N., Gerrity, D., Batista, J., Kim, K.J., Moon, J., 2019. Synthesis, characterization, and kinetic study of activated carbon modified by polysulfide rubber coating for aqueous hexavalent chromium removal. J. Ind. Eng. Chem. 69, 196–210. https://doi.org/10.1016/j.jiec.2018.09.028.

Nagalakshmi, T.V., Emmanuel, K.A., Suresh Babu, C.h., Chakrapani, C.h., Divakar, P.P., 2015. Preparation of Mesoporous Activated Carbon from Jackfruit PPI-1 Waste and Development of Different Surface Functional Groups. International Letters of Chemistry, Physics and Astronomy 54, 189–200. https://doi.org/10.18052/www.scipress.com/ilcpa.54.189.

O'Loughlin, I.B., Kelly, P.M., Murray, B.A., Fitzgerald, R.J., Brodkorb, A., 2015. Concentrated whey protein ingredients: A Fourier transformed infrared spectroscopy investigation of thermally induced denaturation. Int. J. Dairy Technol. 68, 349–356. https://doi.org/10.1111/1471-0307.12239.

Peydayesh, M., Bolisetty, S., Mohammadi, T., Mezzenga, R., 2019. Assessing the Binding Performance of Amyloid-Carbon Membranes Towards Heavy Metal Ions. Langmuir 35, 4161–4170. https://doi.org/10.1021/acs.langmuir.8b04234.

Raj Somera, L., Cuazon, R., Kenneth Cruz, J., Joy Diaz, L., 2019. Kinetics and Isotherms Studies of the Adsorption of Hg(II) onto Iron Modified Montmorillonite/Polycaprolactone Nanofiber Membrane. IOP Conf Ser Mater Sci Eng 540 (1), 012005.

Rajamohan, N., Rajasimman, M., Rajeshkannan, R., Saravanan, V., 2014. Equilibrium, kinetic and thermodynamic studies on the removal of Aluminum by modified Eucalyptus camaldulensis barks. Alex. Eng. J. 53, 409–415. https://doi.org/10.1016/j.aej.2014.01.007.

Ramírez-Rodríguez, L.C., Barrera, L.E.D., Quintanilla-Carvajal, M.X., Mendoza-Castillo, D.I., Bonilla-Petriciolet, A., Jiménez-Junca, C., 2020. Preparation of a hybrid membrane from whey protein fibrils and activated carbon to remove mercury and chromium from water. Membranes (Basel) 10, 1–21. https://doi.org/10.3390/membranes10120386.

Ramírez-Rodríguez, L.C., Quintanilla-Carvajal, M.X., Mendoza-Castillo, D.I., Bonilla-Petriciolet, A., Jiménez-Junca, C., 2022. Preparation and Characterization of an Electrospun Whey Protein/Polycaprolactone Nanofiber Membrane for Chromium Removal from Water. Nanomaterials 12, 2744. https://doi.org/10.3390/NANO12162744/S1.

Rengga, W.D.P., Chafidz, A., Sudibandriyo, M., Nasikin, M., Abasaeed, A.E., 2017. Silver nano-particles deposited on bamboo-based activated carbon for removal of formaldehyde. J. Environ. Chem. Eng. 5, 1657–1665. https://doi.org/10.1016/j.jece.2017.02.033.

Saad, A.H.A., Azzam, A.M., El-Wakeel, S.T., Mostafa, B.B., Abd El-latif, M.B., 2018. Removal of toxic metal ions from wastewater using ZnO@Chitosan core-shell nanocomposite. Environ Nanotechnol Monit Manag 9, 67–75. https://doi.org/10.1016/j.enmm.2017.12.004.

Saleh, T.A., Sari, A., Tuzen, M., 2017. Optimization of parameters with experimental design for the adsorption of mercury using polyethylenimine modified-activated carbon. J. Environ. Chem. Eng. 5, 1079–1088. https://doi.org/10.1016/j.jece.2017.01.032.

Saleh, T.A., Mustaqeem, M., Khaled, M., 2022. Water treatment technologies in removing heavy metal ions from wastewater: A review. Environ Nanotechnol Monit Manag 17, 100617. https://doi.org/10.1016/j.enmm.2021.100617.

Schiesaro, I., Burratti, L., Meneghini, C., Fratoddi, I., Prosposito, P., Lim, J., Scheu, C., Venditti, I., Iucci, G., Battocchio, C., 2020. Hydrophilic Silver Nanoparticles for Hg (II) Detection in Water: Direct Evidence for Mercury-Silver Interaction. J. Phys. Chem. C 124, 25975–25983. https://doi.org/10.1021/acs.jpcc.0c06951.

Selvaraj, R., Prabhu, D., Kumar, P.S., Rangasamy, G., Murugesan, G., Rajesh, M., Goveas, L.C., Varadavenkatesan, T., Samanth, A., Balakrishnaraja, R., Vinayagam, R., 2023. Adsorptive removal of tetracycline from aqueous solutions using magnetic Fe2O3 / activated carbon prepared from Cynometra ramiflora fruit waste. Chemosphere 310, 136892. https://doi.org/10.1016/J.CHEMOSPHERE.2022.136892.

Soroush, S., Mahmoodi, N.M., Mohammadnezhad, B., Karimi, A., 2022. Activated carbon (AC)-metal-organic framework (MOF) composite: Synthesis, characterization and dye removal. Korean J. Chem. Eng. 39, 2394–2404. https://doi.org/10.1007/S11814-022-1100-9/METRICS.

Tran, H.N., You, S.-J., Hosseini-Bandegharaei, A., Chao, H.-P., 2017. Mistakes and inconsistencies regarding adsorption of contaminants from aqueous solutions: A critical review. Water Res. 120, 88–116.

Wang, R., Fan, X.W., Li, Y.Z., 2022. Efficient removal of a low concentration of Pb(II), Fe (III) and Cu(II) from simulated drinking water by co-immobilization between low-dosages of metal-resistant/adapted fungus Penicillium janthinillum and graphene oxide and activated carbon. Chemosphere 286, 131591. https://doi.org/10.1016/j.chemosphere.2021.131591.

Xu, X., Guo, Q., Yang, C., Hu, Z., Chen, Q., Hu, J., 2022. Highly effective removal of Hg (II) solution using corn bract@MoS2 as a new biomass adsorbent. RSC Adv. 12, 31792–31800. https://doi.org/10.1039/D2RA05638K.

Yan, S., Yu, Z., Liu, C., Yuan, Z., Wang, C., Chen, J., Wei, L., Chen, Y., 2020. Dual-Template Pore Engineering of Whey Powder-Derived Carbon as an Efficient Oxygen Reduction Reaction Electrocatalyst for Primary Zinc-Air Battery. Chem. Asian J. 15, 1881–1889. https://doi.org/10.1002/asia.202000399.

Yu, X., Sun, S., Zhou, L., Miao, Z., Zhang, X., Su, Z., Wei, G., 2019. Removing Metal Ions from Water with Graphene-Bovine Serum Albumin Hybrid Membrane. Nanomaterials 9, 276. https://doi.org/10.3390/nano9020276.

Zappone, B., Santo, M.P.D., Labate, C., Guzzi, R., 2013. Catalytic activity of copper ions in the amyloid fibrillation of b-lactoglobulin Bruno. Soft Matter 9, 2412–2419. https://doi.org/10.1039/c2sm27408f.

Zhang, S., Song, J., Du, Q., Cheng, K., Yang, F., 2020b. Analog synthesis of artificial humic substances for efficient removal of mercury. Chemosphere 250, 126606.

Zhang, Q., Zhang, S., Zhao, Z., Liu, M., Yin, X., Zhou, Y., Wu, Y., Peng, Q., 2020a. Highly effective lead (II) removal by sustainable alkaline activated β-lactoglobulin nanofibrils from whey protein. J. Clean. Prod. 255, 1–9. https://doi.org/10.1016/j.jclepro.2020.120297.

Zhao, X., Liu, Y., Shuai, Z., Wang, C., 2019a. Preparation and performance of three-layered structure composite membrane for heavy metal ions and hazardous dyes rejection. Polym. Eng. Sci. 59, E322–E329. https://doi.org/10.1002/pen.24965.

Zhao, Y., Xia, K., Zhang, Z., Zhu, Z., Guo, Y., Qu, Z., 2019b. Facile synthesis of polypyrrole-functionalized CoFe 2 O 4 @SiO 2 for removal for Hg(II). Nanomaterials 9 (3), 455.

Zou, H., Lv, P.F., Wang, X., Wu, D., Yu, D.G., 2017. Electrospun poly(2-aminothiazole)/cellulose acetate fiber membrane for removing Hg(II) from water. J. Appl. Polym. Sci. 134, 2–9. https://doi.org/10.1002/app.44879.

Zúñiga-Muro, N.M., Bonilla-Petriciolet, A., Mendoza-Castillo, D.I., Reynel-Ávila, H.E., Duran-Valle, C.J., Ghalla, H., Sellaoui, L., 2020. Recovery of grape waste for the preparation of adsorbents for water treatment: Mercury removal. J. Environ. Chem. Eng. 8 (3), 103738.